152km-range single-ended distributed acoustic sensor based on in-line optical amplification and micromachined enhanced-backscattering fiber

Ali Masoudi, Martynas Beresna, and Gilberto Brambilla

***Abstract*—In this letter, a distributed acoustic sensor (DAS) with a sensing range in excess of $150km$ is reported. This extended sensing range is achieved by adding an enhanced-backscattering fiber at the far-end of a standard single mode fiber. A conventional DAS system along with inline optical amplifiers are used to interrogate the sensing fiber. The combined system exhibits a minimum detectable strain of $40n\varepsilon$ at 1Hz over a spatial resolution of $5m$.**

The field of distributed acoustic sensing (DAS), also know as distributed vibration sensing (DVS), has experienced a rapid expansion over the past 10 years. This technology which was initially developed for borehole seismic acquisition in oil industry [1] soon found applications in other areas such as damage detection in submarine power cables [2], seismological studies [3], [4] analysis of railway track behavior [5], and highway traffic monitoring [6].

DAS systems with sensing range of up to 40km have proved adequate in areas such as vertical seismic profiling (VSP) and borehole monitoring. However, there are numerous use cases that require DAS systems with much longer sensing range. For instance, the length of high-voltage subsea cables that are used to connect off-shore wind farms to the mainland regularly exceed hundred kilometers and monitoring their health requires DAS with extended sensing range. Even in applications such as perimeter security monitoring or railway track analysis where the sensing fiber can be accessed at regular intervals (e.g. every 35km), using a long-range DAS system might be more cost effective if the cost of infrastructure that is required to host the sensing unit is taken into consideration.

Research on long range DAS systems dates back to 2014 when Wang *et al.* demonstrated an ultra-long phase-sensitive optical time-domain reflectometer (φ-OTDR) system with a 175km sensing range [7]. To achieve this range, the research team used a hybrid distributed amplification consist of co-pumping second-order Raman amplifier and counter-pumping first-order Raman and Brillouin amplifier. The proposed system, however, was an intensity based φ-OTDR capable of qualitative vibration analysis and required access to both ends of the sensing fiber. In 2019, Chen *et al.* added a distributed Raman amplifier to their time-gated digital OFDR (TGD-OFDR) system to demonstrate a quantitative DAS system with 108km of range [8]. The proposed system employed two high power 1455nm lasers at the two ends of the sensing fiber to create a bidirectional Raman amplification. Although the system demonstrated an excellent strain sensitivity of $220p\varepsilon/\sqrt{Hz}$ over 5m spatial resolution, the requirement to access both ends of the sensing fiber restricts the application of this approach in areas where such access is not feasible.

More recently, two studies have demonstrated single-ended DAS systems with sensing ranges in excess of 100km. In 2019, van Putten *et al.* showed that the range of conventional DAS systems can be extended to 100km by adding erbium-doped fibers along the sensing fiber and by remotely pumping them from the front-end of the fiber by a high power 1480nm laser [9]. Using this approach, the team managed to demonstrate a DAS with $100n\varepsilon$ strain sensitivity and 2.5m spatial resolution. In the same year, Cedilnik *et al.* employed an alternative approach to achieve a DAS system with 125km range without using inline amplifiers [10]. Their approach was based on using a combination of Ultra-Low Loss (ULL) fiber and grating-based Enhanced Backscatter Fiber (ENHF) at the front and far-end of the sensing fiber, respectively, in order to reduce the attenuation at the first 90km of the fiber and enhance the back scattered light at the last 5km. While the use of ENHF fibers shown promising results by pushing the sensing range of DAS systems beyond 100km, higher attenuation level of these fibers (~0.7dB/km) limits their use to few kilometers.

Recently, a new class of micro-machined ENHF (μ-ENHF) have been introduced that can boost the backscattered signal without sacrificing the attenuation level of the fiber [11]–[14]. Unlike conventional ENHF fibers which rely on continuous random fiber Bragg grating (FBG) to enhance the backscattered light, μ-ENHF use point reflectors, inscribed at regular intervals, to increase the signal level. With attenuation level similar to that of the conventional telecom fibers, μ-ENHFs can be used to extend the sensing range of DAS system much further compared to what can be achieved with FBG-based ENHF fibers. Furthermore, since the intensity of the reflection at each point can be adjusted independently, the sensing range of DAS fiber can be increased even further by gradually increasing the strength of reflection as a function of distance.

Thus far, researchers have focused on studying how μ-ENHFs can be used to reduce the noise floor of DAS systems to levels well below what can be achieved using conventional optical fibers [12], [13]. In this letter, μ-ENHF is used in conjunction with a conventional DAS interrogator [15] to demonstrate an ultra-long range single-ended DAS system with sensing range in excess of 150km.

The setup used to demonstrate the DAS system with ultra-long sensing range had three main building blocks: 1. DAS interrogator, 2. Inline optical amplifiers, and 3. Low-loss μ-

ENHF. The interrogation setup used in this study is an interferometric DAS system capable of fully quantifying vibrations [16]. The sensing principle of this setup is based on analyzing the phase of the Rayleigh backscattered light from adjacent sections of the sensing fiber. Since Rayleigh scattering is a coherent scattering process, by measuring the difference in the phase of the Rayleigh backscattered light, $\Delta\Phi$, between two points on the fiber and tracking its changes, the variation in the length of the fiber between those two points can be calculated using the following equation [16]:

$$\Delta\Phi = 0.78 \times \frac{4\pi n}{\lambda}\ell + (\varphi_1 - \varphi_2) \tag{1}$$

where n is the effective refractive index of the fiber, λ is the wavelength of the probe light, ℓ is the distance between the two points, and φ_1 and φ_2 are random phases from those points. To measure the phase differences between spatially separated points on the sensing fiber, an imbalanced Mach-Zehnder interferometer (IMZI) with a symmetric 3×3 coupler at its output is employed.The relationship between the phase difference and the intensity of the light at the output of the IMZI is given by [16]:

$$\Delta\Phi = \arctan\left(\frac{\tilde{I}_1 - \tilde{I}_2}{\tilde{I}_3}\right) \tag{2}$$

where $\tilde{I}_1$, $\tilde{I}_2$ and $\tilde{I}_3$ are the AC components of the intensities at the output of the IMZI.

The second major component of the sensing system is the inline optical amplifiers used to enhance the signal level by amplifying both the probe pulse and the backscattered light. The inline optical amplifiers consist of a distributed Raman amplifier and a remotely pumped erbium-doped fiber amplifier (EDFA). Distributed Raman amplification is achieved by launching Raman pump into the sensing fiber along with the probe pulse. The fractional increase in the signal intensity, I_s, driven by pump power P_{pump} is given by [17]:

$$\frac{I}{I_s}\frac{dI_s}{dz} = g_R\, I_{pump} \tag{3}$$

where g_R is the Raman gain coefficient. Although $1450nm$ Raman pump would be the optimal wavelength to maximize the gain at $1550nm$ signal wavelength, a high power $1480nm$ laser is utilized, instead, to both provide distributed Raman gain and act as a pump for the remote EDFA. Remotely pumped EDFA is implemented by splicing a few meters of erbium-doped fiber between two single-mode fiber, each spaning over several tens of kilometers. The residual Raman pump from the first section of the fiber is used to pump the erbium-doped fiber.

The third major element that enables the interrogator to measure acoustic stimulus at such long distance is the μ-ENHF. The properties of μ-ENHF and its fabrication process have been reported in details in [18]. But briefly, a high-power femtosecond laser was synchronized with a custom made rewinding machine to induce localized refractive index (RI) changes at regular intervals along a standard single mode fiber (SSMF). By controlling the exposure time and focal point of the laser, low-loss reflectors with desired reflectivity were formed inside the fiber through fiber polymer coating. The inscription system can be programmed to inscribe reflectors at any point along tens of kilometers of fiber with an accuracy of $1mm$.

The experimental setup for the long-range DAS system is shown in Fig. 1. A narrow linewidth DFB laser diode ($\lambda = 1550nm$, $\Delta\nu = 40kHz$) was used as a seed laser. The laser was intensity modulated by an electro-optic modulator (EOM) to generate $50ns$ probe pulses with a repetition period of $2ms$. The probe pulse was then amplified by an EDFA to reach $50mW$ peak power. To eliminate the forward ASE from the probe pulse, a combination of dense wavelength division multiplexing (DWDM) filter with $100GHz$ bandwidth and acousto-optic modulator (AOM) with an extinction ratio of $50dB$ were used. A 95/5 tap coupler was added at the output of the AOM to monitor the probe pulse.

The distributed Raman amplifier was incorporated into the sensing system by using a 1480/1550nm wavelength division multiplexer (WDM) and a high power $1480nm$ laser. The role of the WDM was to combine the probe pulse with $600mW$ of Raman pump. The power of the pump and the peak power of the probe pulse were adjusted to avoid the onset of non-linear effects such as self-phase modulation.

The common port of the 1480/1550nm WDM was spliced to two $75km$ single-mode fibers (Corning: G.652) joined together by a $4m$-long erbium-doped fiber (FiberCore: M5-980-125). The far-end of the second $75km$ stretch was spliced to $1.2km$-

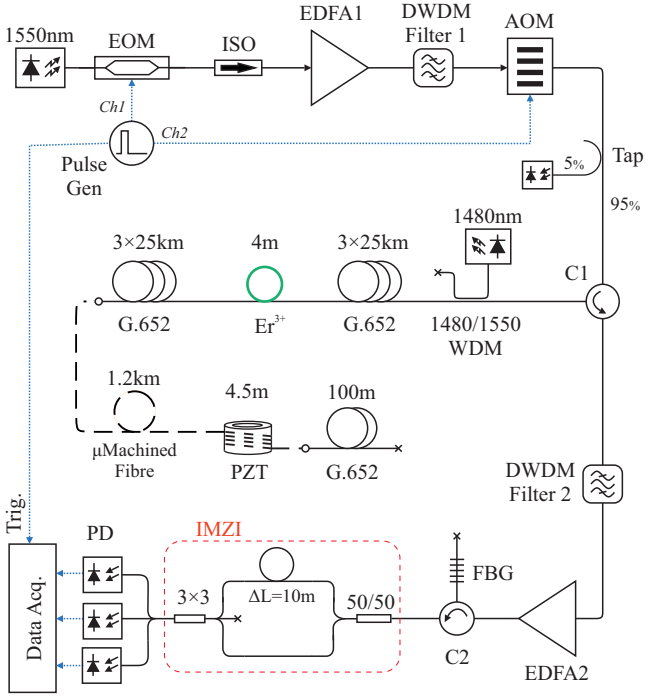

Figure 1. Sensing setup of an ultra long-range DAS system based on remotely pumped EDFA and μ-ENHF. EOM: electro-optic modulator; ISO: isolator; EDFA: erbium-doped fiber amplifier; DWDM: dense wavelength division multiplexing; AOM: acousto-optic modulator; WDM: wavelength division multiplexer; PZT: Piezo-electric actuator; μ-ENHF: Micro-machined Enhanced Backscatter Fiber; FBG: fiber Bragg grating; C: circulator; IMZI, imbalanced Mach–Zehnder interferometer; PD, photodetector; Data Acq.: Data acquisition unit.

long μ-ENHF. The μ-ENHF had around 240 reflectors with $5m$ spacing. The average reflectivity of the reflectors was measured to be $-55dB$. Using cut-back measurement, the attenuation of the μ-ENHF was measured to be $2.02dB/km$ which corresponds to loss of $0.01dB$ per 100 reflectors [12]. Approximately $4.5m$ of the μ-ENHF between 238$^{\text{th}}$ and 239$^{\text{th}}$ reflectors was wrapped around a ring PZT to generate test signals.

The backscattered Rayleigh light from the sensing fiber was first filtered by a second DWDM filter to limit the effect of Raman gain spectrum on the receiving arm of the system to $100GHz$. The signal was then amplified by an optical amplifier (EDFA2) and further filtered by a narrow FBG filter ($\lambda_B = 1550.1nm$, $\Delta\lambda = 5GHz$, Reflectivity = 70%) to remove the ASE and additionally attenuate Raman backscattered light. The amplified backscattered Rayleigh signal was then passed through an IMZI with $10m$ path imbalance and the intensity of the mixed signal at the output of the interferometer was measured by three amplified photodetectors ($BW = 600MHz$, $TIA = 40k\Omega$). The detectors were sampled with a $1GHz$ bandwidth PCIe digitizer at a rate of $625MS/s$.

Figure 2 shows the Rayleigh backscattered trace at the output of the IMZI. From this trace, three zones can be identified: 1) The first zone that covers the first $75km$ of sensing fiber where fractional increase in the signal intensity from the distributed Raman amplification can be observed, 2) The second zone which starts at $0.75ms$, where the erbium-doped fiber is installed, and covers the next $75km$ of the sensing fiber and, 3) The third zone where the μ-ENHF is used and covers the last $1.3km$ of the sensing fiber. The third zone can be identified by its higher signal level as illustrated in the inset of Fig 2.

Figure 3(a) shows the waterfall diagram of the sensing system at the far-end of the sensing fiber. The location of $1Hz$ acoustic stimulus and its profile can be identified on the diagram. The color bar on the diagram indicates the strain level

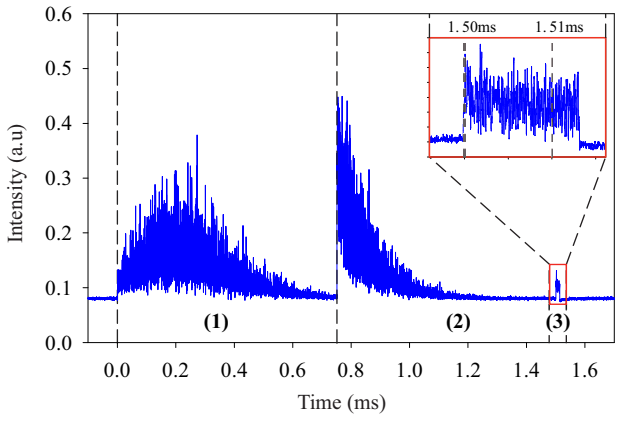

Figure 2. Rayleigh backscattered trace from the sensing fiber collected at the output of the IMZI. Three distinct regions can be identified on the trace: 1) First $750\mu s$ that covers the first section of the sensing fiber with distributed Raman amplification, 2) The period between $750\mu s$ and $1.5ms$ that represents the second section of sensing fibre betwen remotly pumped EDFA and the μ-ENHF, and 3) a $1.3\mu s$ span at the end of the trace that comprises of the μ-ENHF and $100m$ of G.652 fiber.

imposed on the fiber in $\mu\varepsilon$. The width of the stimulated region is $5m$ which corresponds to the distance between the reflectors in μ-ENHF. It should be noted that the spatial resolution of DAS systems that use μ-ENHF to map vibration is dictated by the spatial separation between μ-ENHF reflectors. The comparison of the strain level measured with μ-ENHF and G.652 fiber clearly illustrates that μ-ENHF has much lower noise level. This observation is in agreement with the outcome of previous studies [12], [13].

Figure 3(b) shows strain variation over a $4.5m$ section of the μ-ENHF that is wrapped around the PZT as a function of time. The strain measured by the DAS interrogator, shown in blue circles, agrees with the PZT response to sinusoidal signal which is represented by a red line. The PZT response to input voltage was characterized by a separate MZI arrangement. The signal measured from the μ-ENHF exhibits a more uniform sinusoidal pattern compared with strain measurement based on Rayleigh backscattered light in SSMF [9]. This difference is due to the mechanism in which strain is measured. In conventional fibers, DAS interrogator measures vibration by analyzing the phase of the Rayleigh backscattered light from adjacent points on the sensing fiber. According to eq. (1), the phase difference between any two points is given by the linear term (the first term on the right-hand side of the equation)

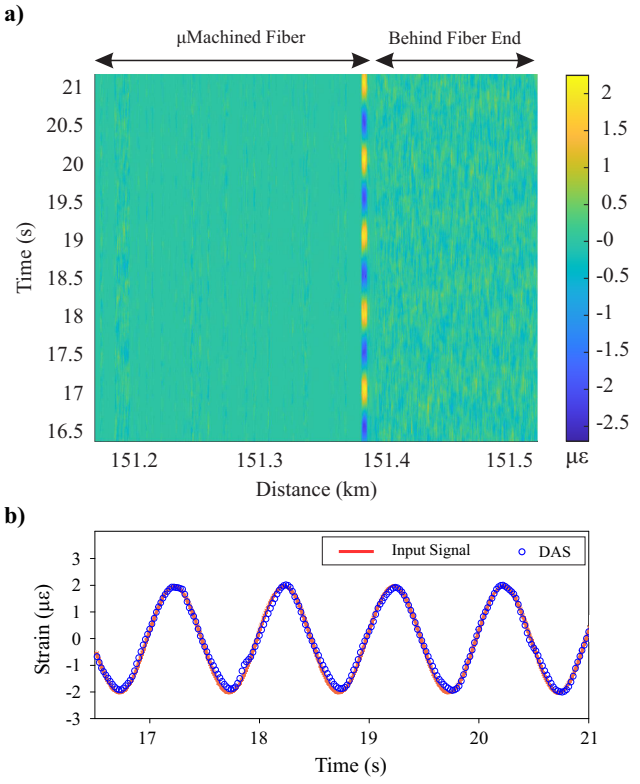

Figure 3. a) Waterfall plot of the sensing system at the far end of the sensing fiber. Each point on the horizontal axis represents the net strain level along a $4m$ section on the sensing fiber. Vibration at each section of the fiber can be analyzed by assessing the changes in the strain level at that point as along the vertical axis. The color bar represents the strain level in $\mu\varepsilon$. b) 2D cross-section of the waterfall plot at a fixed point of the sensing fibre wrapped around the PZT. The blue circles represent the strain measured by DAS while the red line shows the PZT response analyzed by a separate MZI.

which is proportional the distance between those points, ℓ, plus a non-linear term (the second term on the right-hand side of the equation) which is based on the distribution of inhomogeneities in the sensing fiber and changes randomly when the fiber is perturbed [16]. This non-linear term manifest itself as fluctuations in an otherwise uniform sinusoidal signal observed in Ref. [9] results.

In μ-ENHF, on the other hand, vibration is measured by evaluating the phase of the *reflected light* from the point reflectors. Since the reflectors are at single, pre-determined points within the fiber, the phase difference between the light reflected off of any two reflectors is only a function of the distance between them:

$$\Delta\Phi_{\mu Machined} = 0.78 \times \frac{4\pi n}{\lambda}\ell_R \tag{4}$$

where ℓ_R is the distance between two reflectors. The uniformity of sinusoidal pattern seen from the strain measurement by μ-ENHF is attributed to elimination of non-linear term from the phase measurement.

Figure 4(a) shows the PZT-induced strain level measured by the DAS system as a function the input voltage to the PZT. The data points on this plot were obtained by driving the PZT transducer at a fixed frequency over a range of voltages from $500mV$ to $30V$. Minimum strain level detectable at $152km$ was measured to be $40n\varepsilon$ at oscillation frequency of $1Hz$ which corresponds to power spectral density (PSD) of $33n\varepsilon/\sqrt{Hz}$ (Fig. 4(b)). The frequency range of the system was measured to be between $0.1Hz$ to $100Hz$.

In conclusion, a DAS system with a sensing range in excess of $150km$ is demonstrated. This sensing range is achieved by a combination of inline optical amplification and the use of a μ-ENHF with ultra-low loss point reflectors. The sensing system is shown to be capable of quantifying vibrations at the far-end of the sensing fiber with a minimum detectable strain of $40n\varepsilon$ at $1Hz$. The frequency range and spatial resolution of the system were measured to be $0.1Hz \sim 100Hz$ and $5m$, respectively. The authors believe that the sensing range of the proposed system can be extended beyond $200km$ by substituting standard G.652 telecom fiber with ULL pure Silica core fiber and extending the length of μ-ENHF.

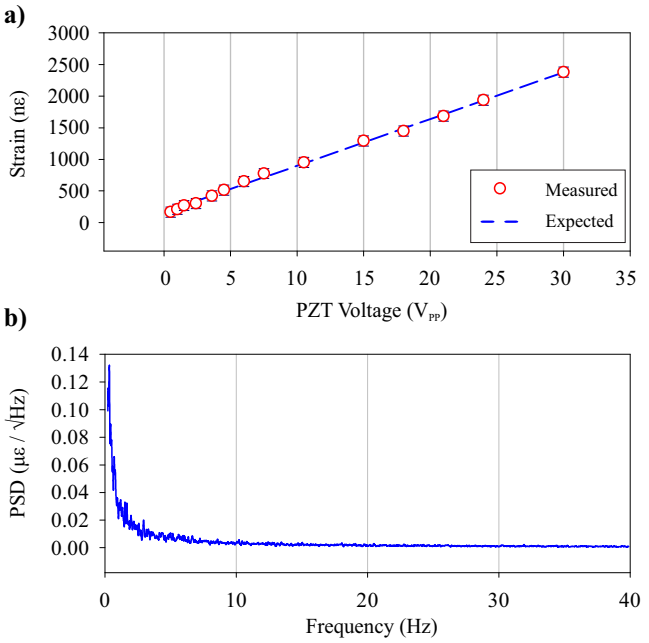

Figure 4. **a)** PZT-induced strain level measured by the DAS system (red circles) as a function the $1Hz$ sinusoidal signal to the PZT. The blue dashed line represents the expected strain level which was obtained through characterization of the PZT transducer by a separate MZI setup. **b)** Power spectral density (PSD) of the DAS system at the far-end of the sensing fiber.

ACKNOWLEDGMENT

The authors would like to thank Sjoerd A.M. Tunissen, Frank G.B.A. Bouwmans, Gijs H.H. Linskens, and Jian Kok for their help in developing the purpose-built rewinding machine and its controllers, David S. Jones, Torran J. Green, and Stafford J. King for developing the image processing and codes to automate the inscription procedure, and Andrei L. Donko for helping in fabrication of μ-ENHF fibers.

FUNDING

Natural Environment Research Council (NE/S012877/1); Royal Society (CHL/R1/180350); Royal Academy of Engineering (PoC1920\21, RF1415\14\6).

REFERENCES

[1] A. Hartog, B. Frignet, D. Mackie, and M. Clark, Geophys. Prospect. **62**, 693-701 (2014).
[2] A. Masoudi, J. A. Pilgrim, T. P. Newson, and G. Brambilla, J. Light Technol. **37**, 1352-1358 (2019).
[3] P. Jousset, T. Reinsch, T. Ryberg, H. Blanck, A. Clarke, R. Aghayev, and C. M. Krawczyk, Nat. Commun. **9**, 1-11 (2018).
[4] N. J. Lindsey, T. C. Dawe, and J. B. Ajo-Franklin, Science **366**, 1103-1107 (2019).
[5] D. Milne, A. Masoudi, E. Ferro, G. Watson, and L. Le Pen, Mech. Syst. Signal. Pr. **142**, 106769 (2020).
[6] S. Xu, Z. Qin, W. Zhang, and X. Xiong, Appl. Sci. **10**, 1839 (2020).
[7] Z. N. Wang, J. J. Zeng, J. Li, M. Q. Fan, H. Wu, F. Peng, L. Zhang, Y. Zhou, and Y. J. Rao, Opt. Lett. **39**, 5866-5869 (2014).
[8] D. Chen, Q. Liu, and Z. He, J. Light Technol. **37**, 4462-4468 (2019).
[9] L. D. van Putten, A. Masoudi, and G. Brambilla, Opt. Lett. **44**, 5925-5928 (2019).
[10] G. Cedilnik, G. Lees, P. E. Schmidt, S. Herstrom, and T. Geisler, IEEE Sens. Lett. **3**, 1-4 (2019).
[11] K. Hicke, R. Eisermann, and S. Chruscicki, Sensors **19**, 4114 (2019).
[12] B. Redding, M. J. Murray, A. Donko, M. Beresna, A. Masoudi, and G. Brambilla, Opt. Express **28**, 14638-14647 (2020).
[13] M. Wu, X. Fan, Q. Liu, and Z. He, Opt. Lett. **44**, 5969-5972 (2019).
[14] A. L. Donko, R. Sandoghchi, M. Beresna, and G. Brambilla, "Low-Loss Micro-Machined Fiber With Rayleigh Backscattering Enhanced By Two Orders Of Magnitude," Optical Fiber Sensors (OFS), **p. WF75** (2018).
[15] A. Masoudi, M. Belal, and T. P. Newson, "Distributed optical fibre audible frequency sensor," Proc SPIE **9157**, 91573T (2014).
[16] M. Chen, A. Masoudi, and G. Brambilla, Opt. Express **27**, 9684 (2019).
[17] A. H Hartog, *An introduction to Distributed Optical Fibre Sensors* (CRC Press, 2017), Chap. 5.
[18] M. Wu, C. Li, X. Fan, C. Liao, and Z. He, Opt. Lett. **45**, 3685-3688 (2020).

REFERENCES

1) Hartog, A., Frignet, B., Mackie, D., & Clark, M. (2014). Vertical seismic optical profiling on wireline logging cable. Geophysical Prospecting, 62(Vertical Seismic Profiling and Microseismicity Frontiers), 693-701.
2) Masoudi, A., Pilgrim, J. A., Newson, T. P., & Brambilla, G. (2019). Subsea cable condition monitoring with distributed optical fiber vibration sensor. Journal of Lightwave Technology, 37(4), 1352-1358.
3) Jousset, P., Reinsch, T., Ryberg, T., Blanck, H., Clarke, A., Aghayev, R., ... & Krawczyk, C. M. (2018). Dynamic strain determination using fibre-optic cables allows imaging of seismological and structural features. Nature communications, 9(1), 1-11.
4) Lindsey, Nathaniel J., T. Craig Dawe, and Jonathan B. Ajo-Franklin. "Illuminating seafloor faults and ocean dynamics with dark fiber distributed acoustic sensing." Science 366.6469 (2019): 1103-1107.
5) Milne, D., Masoudi, A., Ferro, E., Watson, G., & Le Pen, L. (2020). An analysis of railway track behaviour based on distributed optical fibre acoustic sensing. Mechanical Systems and Signal Processing, 142, 106769.
6) Xu, S., Qin, Z., Zhang, W., & Xiong, X. (2020). Monitoring Vehicles on Highway by Dual-Channel φ-OTDR. Applied Sciences, 10(5), 1839.
7) Wang, Z. N., J. J. Zeng, J. Li, M. Q. Fan, H. Wu, F. Peng, L. Zhang, Y. Zhou, and Y. J. Rao. "Ultra-long phase-sensitive OTDR with hybrid distributed amplification." Optics letters 39, no. 20 (2014): 5866-5869.
8) Chen, Dian, Qingwen Liu, and Zuyuan He. "108-km Distributed Acoustic Sensor With 220-p$\epsilon/\sqrt{Hz}$ Strain Resolution and 5-m Spatial Resolution." Journal of Lightwave Technology 37, no. 18 (2019): 4462-4468.
9) van Putten, L. D., Masoudi, A., & Brambilla, G. (2019). 100-km-sensing-range single-ended distributed vibration sensor based on remotely pumped Erbium-doped fiber amplifier. Optics Letters, 44(24), 5925-5928.
10) Cedilnik, G., Lees, G., Schmidt, P. E., Herstrom, S., & Geisler, T. (2019). Pushing the Reach of Fiber Distributed Acoustic Sensing to 125 km Without the Use of Amplification. IEEE Sensors Letters, 3(3), 1-4.
11) Hicke, Konstantin, Rene Eisermann, and Sebastian Chruscicki. "Enhanced distributed fiber optic vibration sensing and simultaneous temperature gradient sensing using traditional C-OTDR and structured fiber with scattering dots." Sensors 19, no. 19 (2019): 4114.
12) Redding, Brandon, Matthew J. Murray, Andrei Donko, Martynas Beresna, Ali Masoudi, and Gilberto Brambilla. "Low-noise distributed acoustic sensing using enhanced backscattering fiber with ultra-low-loss point reflectors." Optics Express 28, no. 10 (2020): 14638-14647.
13) Wu, Mengshi, Xinyu Fan, Qingwen Liu, and Zuyuan He. "Quasi-distributed fiber-optic acoustic sensing system based on pulse compression technique and phase-noise compensation." Optics Letters 44, no. 24 (2019): 5969-5972.
14) Donko, Andrei, Reza Sandoghchi, Martynas Beresna, and Gilberto Brambilla. "Low-Loss Micro-Machined Fiber With Rayleigh Backscattering Enhanced By Two Orders Of Magnitude." In Optical Fiber Sensors, p. WF75. Optical Society of America, 2018.
15) Masoudi, Ali, Mohammad Belal, and Trevor P. Newson, "Distributed optical fibre audible frequency sensor," Proc SPIE **9157**, 91573T (2014).
16) Chen, Mengmeng, Ali Masoudi, and Gilberto Brambilla. "Performance analysis of distributed optical fiber acoustic sensors based on φ-OTDR." Optics express 27, no. 7 (2019): 9684-9695.
17) A. H Hartog, *An introduction to Distributed Optical Fibre Sensors* (CRC Press, 2017), Chap. 5.
18) Wu, Mengshi, Chi Li, Xinyu Fan, Changrui Liao, and Zuyaun He. "Large-scale multiplexed weak reflector array fabricated with a femtosecond laser for a fiber-optic quasi-distributed acoustic sensing system." Optics Letters 45, no. 13 (2020): 3685-3688.